

Isometric embeddings of 2-spheres by embedding flow for applications in numerical relativity

Michael Jasiulek* Mikołaj Korzyński †

February 19, 2022

Abstract

We present a numerical method for solving Weyl’s embedding problem which consists of finding a global isometric embedding of a positively curved and positive-definite spherical 2-metric into the Euclidean three space. The method is based on a construction introduced by Weingarten and was used in Nirenberg’s proof of Weyl’s conjecture. The target embedding results as the endpoint of an embedding flow in \mathbf{R}^3 beginning at the unit sphere’s embedding. We employ spectral methods to handle functions on the surface and to solve various (non)-linear elliptic PDEs. Possible applications in 3 + 1 numerical relativity range from quasi-local mass and momentum measures to coarse-graining in inhomogeneous cosmological models.

1 Introduction

It is a classic result in differential geometry that for every 2-surface of S^2 topology, equipped with a positive-definite metric whose curvature is positive, a global isometric embedding into the Euclidean three space can be found. Moreover, the embedding is unique up to the isometries of the target Euclidean space which are rigid motions: rotations and translations as well as reflections [9, 18]. This was conjectured by Hermann Weyl and later proven by Alexandrov and Pogorelov [1, 17], and independently by Nirenberg [15].

Isometric embeddings into flat space have a wide range of applications in general relativity. For a given isometric embedding in a curved ambient space they provide a reference surface, thereby fixing the intrinsic geometries. From the difference between the extrinsic geometries it is possible to define measures of quasi-local mass like the Brown-York and Kijowski-Liu-Yau masses [11, 3, 4, 14]. For more examples see Szabados’ review article [19]. Such quasi-local mass measures – not yet applied in (3+1) numerical relativity – could potentially be useful

*Max-Planck-Institut für Gravitationsphysik (Albert-Einstein-Institut), Am Mühlenberg 1, D-14476 Potsdam, Germany, E-mail: michaelj@aei.mpg.de

†Gravitational Physics, Faculty of Physics, University of Vienna, A-1090 Vienna, Austria, E-mail: mikolaj.korzynski@univie.ac.at

to determine mass and momenta in binary black hole simulations. In addition, the uniqueness of the reference shapes makes them ideal for visualising 2-metrics. Another application can be found in 3+1 numerical cosmology, where isometric embeddings of S^2 surfaces are the principle step in a method for coarse-graining (averaging) of expansion and shear in inhomogeneous cosmological models proposed by MK in [13, 12].

The isometric embedding equations constitute a three-dimensional (3D) non-linear, coupled system of PDEs, for which standard numerical methods can not be applied and analytical solutions are impossible to find. This could be a reason why no practical application in numerical simulations exists. The problem has already been addressed twice: by Nollert and Herold in [16], and by Bondarescu, Alcubierre and Seidel [2]. In the algorithm presented in [16], the surface in question is triangulated and then a corresponding polyhedron in \mathbf{R}^3 is constructed, whose edges have a length approximating those of the source triangulation. The method has a serious drawback: multiple polyhedra exist fulfilling the length constraints between neighboring points, most of them converge to unwanted non-regular (non-differentiable) surfaces. For the method in [2] the three unknown embedding functions are expanded into harmonic polynomials of maximal degree l_{\max} and the embedding problem is turned into a numerical minimization problem of a $3(l_{\max} + 1)^2$ dimensional functional, which vanishes only if the embedding is isometric. This renders the method crucially dependent upon the minimisation algorithm used which, among other things, must steer away from the false minima of the functional. The minimization becomes increasingly difficult and computationally costly by increasing the dimensionality of the parameter space.

Our algorithm is based on the continuity method used in Nirenberg's proof and is not effected by the aforementioned problems. Its convergence to the right solution is guaranteed by Nirenberg's theorem. The target embedding results as the final surface of an embedding flow beginning with the unit sphere's embedding in \mathbf{R}^3 . In each step of the flow the solution of the linearised embedding equation (LEE) allows one to continuously deform the surface from a round unit sphere to the final shape. This requires the conformal factor linking target and spherical round 2-metric, which we obtain as a steady-state solution of the Ricci flow. However we note that, unlike the previous two approaches, it is strictly limited to surfaces whose curvature is positive everywhere: Even if the isometric embedding exists for a surface with non-positive curvature, the algorithm can not be applied.

We present a variety of numerical methods, among others, a pseudo-spectral parabolic evolution scheme to solve the various elliptic PDEs appearing in the problem that could be interesting for other purposes in numerical relativity.

The paper is organized as follows: In the next section we provide the mathematical background for the paper, as well as description of the linearized embedding flow we use. In the third section we discuss the technical details of the algorithm and its implementation; in the fourth, we present the results of a concrete numerical test case. We state the final conclusions in the fifth section and in the appendix, where we also quote relevant but more technical results

obtained in this paper.

2 The mathematical background

The Weyl problem can be described as follows: Given a 2-surface C of spherical topology, equipped with a positive-definite metric q (target metric), find a sufficiently regular embedding into the Euclidean space

$$\Phi : C \rightarrow \mathbf{R}^3 \tag{1}$$

which preserves the 2-metric q , i.e.

$$q = \Phi^* \delta \tag{2}$$

where δ is the standard metric on \mathbf{R}^3 and Φ^* denotes the standard pullback. In this paper we shall assume that the metric and the embedding are smooth.

It is known that the embedding always exists if the metric is sufficiently regular and its curvature is positive everywhere [15, 9]. It is also known to be unique up to the rotations, translation and reflexions in the Euclidean space (see for example [18] for a review of the rigidity results).

The algorithm to determine Φ , which we present in this paper, is based on the continuity method used in Nirenberg's proof of existence and introduced by Weyl. It consists of three steps which we will now describe briefly, leaving their detailed discussion until the next subsections.

At first we compute the conformal factor relating the target metric to the metric of the round sphere with radius one 0q (round metric) which is a steady-state solution of the Ricci flow.

$${}^0q = e^{-2\sigma} q \tag{3}$$

It is known that the Ricci flow uniformizes the metric [8], i.e. the flow converges to a constant curvature metric $q \rightarrow {}^0q$ whereby we obtain σ . In general, the round metric and σ are then given in arbitrary coordinates. This has to be corrected through a transformation, for which the coordinate representation of 0q and its embedding Φ_0 into \mathbf{R}^3 take a standard well-known form.

Then we construct a one-parameter family of metrics

$${}^tq = \Omega(t, \sigma)^2 {}^0q, \tag{4}$$

where $\Omega(t, \sigma)$ is a function chosen such that ${}^{t=1}q$ is the target metric and ${}^{t=0}q$ the round metric, which allows one to morph one metric smoothly into the other.

Finally, we perform the embedding flow: Beginning at $t = 0$ the known standard embedding Φ_0 of the round metric is deformed in 'small' steps such that the induced metric of the deformed surface at each step matches tq until the target metric is reached. This is accomplished by solving the linearized embedding equations, which relate a small change of the metric tensor with a small deformation of the embedding functions.

We now proceed to describe the three steps in detail.

2.1 The Ricci flow

In the first step of our method we have to determine the conformal factor between the target and round sphere metric. In Riemannian 2-manifolds the Ricci flow reduces to a single equation for the conformal factor

$$\begin{aligned} p(\tau) &= q e^{-2\rho(\tau)} \\ \dot{\rho} &= \mathcal{R}[p(\tau)] - \langle \mathcal{R}[p(\tau)] \rangle, \end{aligned} \quad (5)$$

where $\mathcal{R}[p]$ is the Ricci scalar of the metric p and $\langle \mathcal{R}[p] \rangle$ its surface average wrt q included to keep the surface area of p bound. $\mathcal{R}[p]$ is related to the Ricci scalar of the target metric in the following way

$$\mathcal{R}[p] = e^{2\rho}(\mathcal{R}[q] + 2 {}^q\Delta\rho), \quad (6)$$

with ${}^q\Delta$ being the Laplacian wrt to q .

The flow converges for large τ to a function $\rho \xrightarrow{\tau \rightarrow \infty} \sigma$ for which $e^{-2\sigma} q$ is a round sphere metric (see [6, 8], the latter also in [5]). By simple rescaling of σ we can ensure that the sphere has the area of 4π . Now it is possible to construct a family of metrics joining target and round sphere metric

$${}^tq = {}^0q \Omega(t, \sigma)^2. \quad (7)$$

where $\Omega(t, \sigma)$ should be chosen such that $\mathcal{R}[{}^tq]$ is always positive. This is guaranteed for $\Omega(t, \sigma) = e^{2\sigma t}$. We have also tested a different function to drive the embedding flow $\Omega(t, \sigma) = t(e^\sigma - 1) + 1$, in which the change between consecutive embeddings in the flow, as explained later, is linear in t as well.

2.2 Round metric in standard coordinates

The steady-state solution of the Ricci flow is a round metric ${}^0q = e^{-2\sigma} q$ in arbitrary coordinates. To proceed, a transformation to standard coordinates x^i is required for which its isometric embedding X^i into \mathbf{R}^3 takes the well-known form, unique up to rotations and reflections

$$\begin{aligned} X^1 &= x/r = \sin \theta \cos \varphi \\ X^2 &= y/r = \sin \theta \sin \varphi \\ X^3 &= z/r = \cos \theta, \end{aligned} \quad (8)$$

where $r = \sqrt{x^2 + y^2 + z^2}$ and (θ, φ) are spherical coordinates corresponding to x^i . Note that the three functions on the right hand side of (8) constitute a real, orthogonal basis for the spherical harmonics with $l = 1$. This means that these functions, denoted as n^i , are eigenfunctions of the Laplace operator on the sphere with eigenvalue -2

$$\Delta n^i = -2n^i, \quad i = 1, 2, 3. \quad (9)$$

They are also orthogonal and normalized in the sense that

$$\oint_C n_i n_j dA = \frac{4\pi}{3} \delta_{ij}, \quad (10)$$

where dA is the area element associated with the round metric. It is easy to check that the opposite is also true: Any three orthogonal and properly normalized functions satisfying (9) are related to (8) by an $O(3)$ linear mapping and therefore constitute an isometric embedding of the unit sphere themselves. Equation (9) in turn can be solved numerically even in non-standard coordinates.

2.3 The linearized embedding equation

Consider an S^2 surface D , endowed with a coordinate system θ^A and embedded in \mathbf{R}^3 by a mapping described by three functions $X^i(\theta^A)$. The induced metric has the form of

$$q_{AB} = X^i_{,A} X^j_{,B} \delta_{ij}. \quad (11)$$

If we deform the embedding by adding a small $\delta X^i(\theta^A)$, the metric changes according to

$$\delta q_{AB} = 2 \delta X^i_{(A} X^j_{,B)} \delta_{ij} \quad (12)$$

up to the linear order. Given the metric change δq one can ask for the compatible deformation vector. Finding δX^i involves solving (12), which is called the linearized embedding equations (LEE). Through a variable transformation this linear system of three PDEs can be turned into to a single elliptic equation of the second order for Weingarten's "Verschiebungsfunktion" and two ODEs, see also [9, 15] for derivations. Let Y^i denote the deformation vector field we seek and d_{ij} the metric deformation and let s^i be the outward-pointing null normal. We decompose Y^i into the normal and tangential part:

$$Y^i = \Upsilon s^i + I^i \quad (13)$$

and introduce new variables u_A and w

$$\begin{aligned} u_A &= s_k Y^k_{,A} \\ w &= -\epsilon^{AB} D_A I_B. \end{aligned}$$

ϵ^{AB} denotes the area form and D_A is the covariant derivative on the surface. Y^i can be reconstructed from u_A and w via

$$\begin{aligned} \Upsilon_{,A} &= u_A - K_{AB} I^B \\ D_A I_B &= -\frac{1}{2} w \epsilon_{AB} + \frac{1}{2} d_{AB} + \Upsilon K_{AB}, \end{aligned} \quad (14)$$

where K_{AB} denotes the extrinsic curvature. On a surface of positive scalar curvature K_{AB} is positive definite ¹ and therefore has an inverse $(K^{-1})^{AB}$. The variable u_A is then related to the first derivative of w by

$$\begin{aligned} u_A &= \frac{1}{2} \epsilon_{AB} (K^{-1})^{BD} (c_D - w_{,D}), \\ c_D &= -D_A q_{BD} \epsilon^{AB}. \end{aligned} \tag{15}$$

Finally w itself has to satisfy an elliptic equation

$$\mathcal{L}w = \tau. \tag{16}$$

The elliptic operator \mathcal{L} is defined as

$$\mathcal{L}w = D_A ((K^{-1})^{AB} w_{,B}) + \mathcal{K}w, \tag{17}$$

where $\mathcal{K} = K^A{}_A$, and the right hand side of the equation is

$$\tau = D_A ((K^{-1})^{AB} c_B) - K^C{}_A d_{BC} \epsilon^{AB}. \tag{18}$$

Equation (16), together with (15) and (14), is equivalent to the original LEE.

\mathcal{L} is self-adjoint with the standard scalar product $\langle f, g \rangle = \int_C f^* g \, dA[q(t)]$ and thus has only real eigenvalues. Moreover, for any convex surface it has a three-dimensional kernel spanned by the components of the normal vector $s^1(\theta^A)$, $s^2(\theta^A)$ and $s^3(\theta^A)$ [9]. In case of a round sphere it is possible to demonstrate that $\mathcal{L} = \Delta + 2$.

Since \mathcal{L} has a non-trivial kernel, it is not invertible. Nevertheless, equation (16) has solutions if its right hand side is orthogonal to the kernel:

$$\langle \tau, s^i \rangle = 0. \tag{19}$$

The solution is unique up to adding a combination of the functions s^i , $i = 1, 2, 3$. Geometrically this ambiguity corresponds to the possibility of adding a rigid rotation generator to solutions of (12).

3 Technical and numerical details

In this section we explain the numerical and technical details of our implementation. Our approach consists of three main steps: the Ricci flow to relate target and round metric, the $l = 1$ eigenvalue problem of the round metric Laplacian in non-standard coordinates, and the embedding flow from the round metric's embedding to the target embedding. For each computational step we need to conduct a variety of high accuracy numerical operations on spherical surfaces (numerical integration, interpolation, (anti)-differentiation, coordinate inversion, solving elliptic PDEs). For this reason spectral methods in combination with particular coordinates are the best choice as we explain in the following.

¹This is the precise reason why our method is limited to positively curved metrics.

3.1 Coordinate basis, polynomial basis, grid setup

Instead of covering spherical surfaces with 2D coordinate maps we consider 2-surfaces as being embedded in some (fictitious) ambient Riemannian 3-space (for example the Euclidian space), equipped with some 3D quasi-Cartesian coordinate system $\{\hat{x}^i\}$ and represent all surface tensors using this exterior coordinate basis. Polar coordinates $(\hat{\theta}, \hat{\phi})$ on the surface are merely used to label the grid points $(\hat{\theta}_i, \hat{\phi}_j)$, $i = 1, \dots, N_{\hat{\theta}}$, $j = 1, \dots, 2N_{\hat{\theta}}$. We use a Gauss-Legendre grid structure, the *canonical* grid, on which a surface integral of polynomials of degree $2l_{\max} = 2(N_{\hat{\theta}} - 1)$ can be represented exactly by a finite sum.

Our approach requires various numerical operations on the surface: function evaluations at non-canonical points (“eval”), numerical integration, function inversion (“inv”), differentiation and anti-differentiation (“int”). For this reason we chose to represent the shape function h and other surface tensors as an expansion in harmonic polynomials.

$$h = \sum_{lm}^{l_{\max}} \Phi[h]^{lm} \Phi^{lm} + \mathcal{O}(l_{\max} + 1) = \sum_{lm}^{l_{\max}} Y[h]^{lm} Y^{lm} + \mathcal{O}(l_{\max} + 1), \quad (20)$$

where Y^{lm} is the standard orthonormalised basis and the other basis is defined by $\Phi^{lm} := (\hat{n}^i \mathcal{N}_i^{lm})^l$, where $\hat{n}^i = \hat{x}^i / \hat{r} = (\sin \hat{\theta} \cos \hat{\phi}, \sin \hat{\theta} \sin \hat{\phi}, \cos \hat{\theta})$ is the radial unit normal. This basis is orthogonal wrt distinct l -eigen-spaces. \mathcal{N}_i is a list of constant complex null vectors that span the $2l + 1$ harmonics in each eigenspace. The null vectors are chosen as in [10], then both basis are related by a discrete Fourier transform in each eigenspace.

3.2 Differentiation on the surface

The simple form of the basis $(n^i \mathcal{N}_i^{lm})^l$ is practical for evaluation of functions off the grid. In addition its differentiation² is straightforward, for example the derivative in 3d coordinates takes the form of

$$\partial_i h = \partial_i n^k \sum_{lm} \Phi[h]^{lm} (n^j \mathcal{N}_j^{lm})^{l-1} l \mathcal{N}_k^{lm}. \quad (21)$$

By placing $\partial_i n^k \rightarrow \partial_{\theta} n^k$ in front of the sum above, one obtains $\partial_{\theta} h$ etc.; another practical feature.

We prescribe 2-surfaces through level set functions G / shape functions h , see fig. (1) (left), in some ambient manifold (Σ, γ_{ij}) , as is common in numerical simulations of the Einstein equation in (3+1) dimensions. If a shape function h is given, the computational steps to calculate curvature tensors on the surface are as follows

$$h \rightarrow [h]^{lm} \rightarrow \begin{array}{l} \partial_i h, \partial_{ij} h \\ \partial_{ijk} h \end{array} \rightarrow \begin{array}{l} s_i, q_{ij}, K_{ij} \\ \partial_i K_{jk} \end{array} \rightarrow \begin{array}{l} \mathcal{R}, K_{ij}^{(-1)} \\ \partial_i K_{jk}^{(-1)} \end{array}, \quad (22)$$

²Alternatively, the differentiation of an expansion in Y^{lm} s can be performed by evaluating $\partial_i, \partial_{ij} Y^{lm}$ from $\partial_i, \partial_{ij} \Phi^{lm}$. It is practical to tabulate the $\partial_i, \partial_{ij} Y^{lm}$ initially.

where the expressions in blue are only necessary for solving the LEE.

The computation of curvature tensors on the surface requires ${}^qD_i\chi_j$ of tensors χ_i , which might have a normal component $\chi_s \neq 0$, as for example $\partial_i h$,

$${}^qD_i\chi_j = ({}^\gamma D_i\chi_j)^\parallel - K_{ij}\chi_s, \quad (23)$$

which is not simply the tangential part of the ambient derivative $({}^\gamma D_i\chi_j)^\parallel$. As a consequence, the Laplacian of a function ψ on C is calculated by

$${}^q\Delta\psi = q^{ij}\partial_{ij}\psi - \gamma\Gamma^i\partial_i\psi - \mathcal{K}\partial_s\psi, \quad (24)$$

where $\gamma\Gamma^i = \gamma\Gamma_{jk}^i q^{jk}$ is this contraction with the Christoffel symbols of γ_{ij} .

3.3 Parabolic flow relaxation method

The elliptic PDEs of type $\mathcal{L}(u) - V(u) = 0$ appearing in our approach are solved by considering the associated parabolic flow equation ³

$$\dot{u} = \mathcal{L}(u) - V(u) \xrightarrow{-\langle \text{rhs} \rangle} \dot{u} = \{\mathcal{L}(u) - V(u)\}^{/l=0} \quad (25)$$

where \dot{u} is the time derivative of u and $\{\bullet\}^{/l=0} := \bullet - \langle \bullet \rangle$ removes a function's surface average ($l = 0$ mode). For linear elliptic operators \mathcal{L} with a non-positive spectrum, except $l = 0$, arbitrary initial data evolves to a steady-state solution (at $\dot{u}, \ddot{u}, \dots = 0$) of the parabolic PDE which is automatically a solution to the elliptic equation. The Ricci flow is a parabolic PDE with a non-linear elliptic part. The existence of its steady states and convergence to them is known [6, 8].

The parabolic PDEs we deal with are solved by means of a pseudo-spectral scheme, where we use the method of lines, 2. or 4. order Runge-Kutta (RK2, RK4) and spectral finite difference methods, see eq. (21), until $|\dot{u}|$ falls below machine/spectral precision. Since we are not interested in the details of the solution during the relaxation period, but in a quick fall-off, we pick a coarse time-step Δt and RK2 (Heun), where we take the CFL-condition of the heat equation with explicit Euler $\Delta t < \nu(\Delta x)^2$, $\nu = 0.25$ as an orientation.

The algebraic operations to compute the rhs produce an aliasing error. Therefore, we filter modes $> l_{\max}$ from the rhs.

3.4 Computational steps: Ricci flow, EVP, LEE

The computational steps of the main component 'Ricci flow' of our implementation are the following. A shape function $h(\hat{x})$ and an ambient geometry, see fig. (1) (left), are required as input

³ In principle, the spectral decomposition of functions on the surface would allow us to turn non-linear / linear elliptic PDEs into algebraic / linear systems of equations to be solved with Newton-Raphson's / splitting (relaxation) methods which are numerically more efficient but more stringent with regard to the initial guess and the conditioning of involved matrices. The parabolic flow relaxation method on the other hand covers non-linear / linear elliptic PDEs and is more robust. Moreover, efficiency is not a concern for the 2D PDEs we deal with.

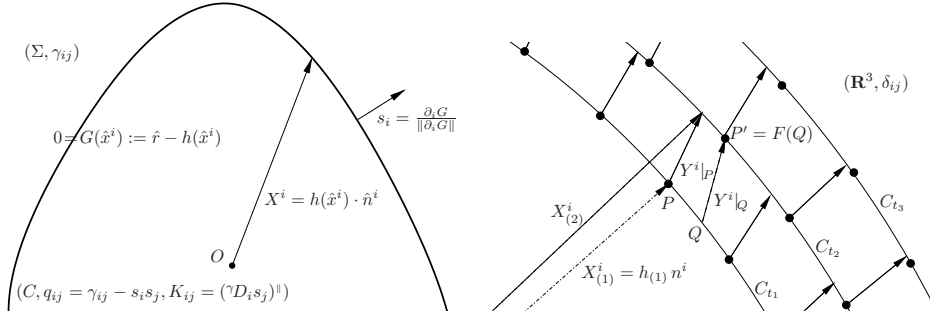


Figure 1: Left: Level surface (C, q_{ij}) given by $G(\hat{x}^i) = \hat{r} - h(\hat{x}^i)$ at $G = 0$ and induced metric q_{ij} in the Riemannian manifold (Σ, γ_{ij}) . Right: Embedding flow at $t = t_1, t_2, t_3$ in the Euclidean space. Shift vector field Y^i at each step induces a new embedding $F : X_{(1)}^i \mapsto X_{(2)}^i = X_{(1)}^i + Y^i$ that is in general off the canonical grid (dots).

$$h(\hat{x}) \rightarrow \text{eq. (22)} \rightarrow \text{evolve: } \dot{\sigma} = \{\mathcal{R}[e^{2\sigma} q]\}^{/l=0} \rightarrow \sigma(\hat{x}), {}^0q(\hat{x})_{ij},$$

where $\mathcal{R}[e^{2\sigma} q] = e^{2\sigma} (\mathcal{R}[q] + 2 {}^q\Delta\sigma)$ and ${}^q\Delta\sigma$ is computed as in eq. (24). The spherical round metric ${}^0q_{ij} = e^{-2\sigma} q_{ij}$ with $\mathcal{R}[{}^0q] \equiv 2$ is the steady-state solution of the Ricci flow. It is given in non-standard coordinates in which its Laplacian takes the form ${}^0\Delta\bullet = e^{2\sigma} {}^q\Delta\bullet$. As a standard coordinate basis, we take the three orthonormalised $l = 1$ eigenfunctions n^j of ${}^0\Delta$, see eq. (8)

$$\sigma(\hat{x}) \rightarrow \text{evolve: } \dot{n}^i = \{{}^0\Delta n^i + 2n^i\}^{/l=0} \rightarrow n^j(\hat{x}) \xrightarrow{\text{inv}} \hat{n}^i(x) \xrightarrow{\text{eval}} \sigma(x)$$

in which 0q takes the well known simple form ${}^0q_{ij} = \delta_{ij} - n_i n_j$. Identifying x^i with Cartesian coordinates in \mathbf{R}^3 maps ${}^0q_{ij}, \sigma$ to the Euclidean space where the embedding flow is performed, see fig. (1) (right). We construct a family of metrics ${}^tq_{ij} = \Omega(t, \sigma)^2 \cdot {}^0q_{ij}$ such that ${}^{t=0}q \equiv {}^0q$ and ${}^{t=1}q \equiv q$ with $\mathcal{R}[{}^tq] > 0$ and divide the time interval into N steps, i.e. $t = 0, t_1, t_2, \dots, t_N$ ⁴ whereby we slowly deform tq into the target metric so that the difference

$${}^{(n)}d_{ij} := q(t_{n+1})_{ij} - {}^{(n)}q_{ij} \quad (26)$$

is small, where ${}^{(n)}q_{ij}$ is the induced metric wrt $h_{(n)}$, see fig. (1) (left), at the n th step. We initialize the flow with the shape function $h_{(0)} = 1$ corresponding to the standard embedding of the unit sphere. At every step we compute

$$\begin{aligned} h_{(n)} &\rightarrow \text{eq. (22)} \rightarrow \text{compute: } {}^{(n)}d_{ij} \rightarrow \text{evolve: } \dot{w} = \{(\mathcal{L}(w) - \tau)/\mathcal{K}\}^* \\ &\rightarrow w \xrightarrow{\text{int}} Y^i|_P \rightarrow n_{(n+1)}^i(x|_P) \xrightarrow{\text{inv}} n^i(x_{(n+1)}|_{P'}) \xrightarrow{\text{eval}} (Y^i, \partial_j Y^i, \sigma, q_{ij})|_Q \\ &\rightarrow (h_{(n+1)}, q_{ij})|_{P'}, \end{aligned}$$

⁴The number of steps and the values t_n are arbitrary and depend on how far q is off the round metric, usually $3 < N < 7$.

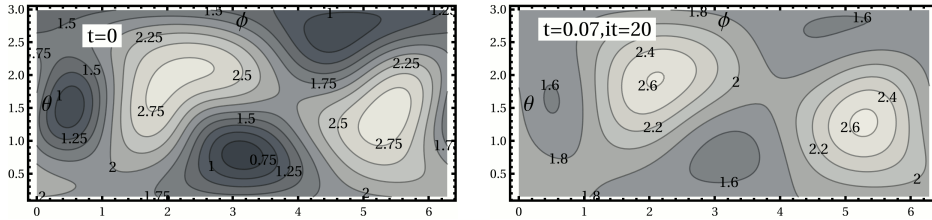


Figure 2: (θ, ϕ) -contour plots of the scalar curvature $\mathcal{R}[tq]$ in relaxation flow at $t = 0$ and $t = 0.07$.

where $*$ denotes projecting out the lowest eigenvalue of \mathcal{L} (see Appendix). The complications arise from the fact that the new embedding induced by Y^i is shifting the points off the canonical grid, moreover, the target metric (0q and σ) has to be transported under the mapping $X_{(n+1)}^i = X_{(n)}^i + Y^i$ from one surface to the other.

$$q_{ij}|_{P'} = \frac{\partial X_{(n)}^k}{\partial X_{(n+1)}^i} \frac{\partial X_{(n)}^l}{\partial X_{(n+1)}^j} q_{kl}|_Q \quad (27)$$

After N equi-distant steps $h_{(N)}$ the difference (26) between the target metric and the induced metric wrt $h_{(N)}$ is of the order $N \cdot \mathcal{O}(d)$. But this solution can be refined by recursively applying ⁵the above computational steps with ${}^{t=1}q_{ij}$ fixed in eq. (26) whereby d_{ij} converges to zero exponentially.

4 Numerical test case

In this section we apply our procedure to a numerical test case, where we prescribe a test shape function in the Euclidean space given by the function below. We solve the embedding problem numerically and compare the original embedding with the resulting one. More specifically, we compute the induced 2-metric, perform the Ricci flow to the round sphere, solve the EV problem and perform the embedding flow from the round sphere to the target shape, solving the linearized embedding equation at each step.

As a test case we pick a cigar-shaped function (for illustration purposes) and add a randomized non-polynomial part

$$h = c_1 \left(1 + c_2 \text{Re}[(\mathcal{N}_1^j n_j)]^2 + \sqrt{1 + c_3 \text{Re}[(\mathcal{N}_2^j n_j)^2 + (\mathcal{N}_3^j n_j)^3]} \right)$$

$c_{1,2,3} = 0.458, 0.5, 0.15$ (for which the area $A \approx 1$ and $\mathcal{R} > 0, \mathcal{K} > 0$) and $\mathcal{N}_{1,2,3}$ ⁶are three randomly oriented null vectors. This way all lm modes are occupied in a somewhat random manner. The surface defined by this shape function has

⁵If necessary this refinement process can be applied at any intermediate time t_n , such that the embedding flow does not move to far off the conformal metric flow.

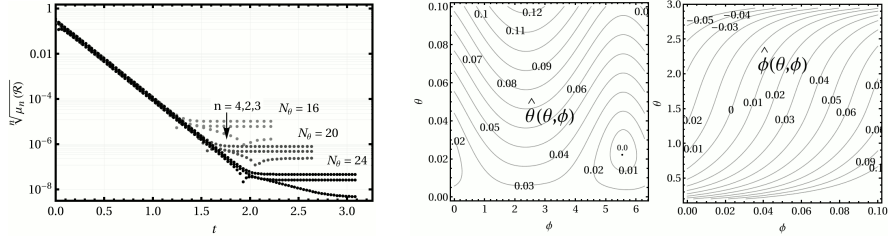


Figure 3: Left: Exponential fall-off of $n\sqrt{\mu_n(\bar{\mathcal{R}})}$ for $n = 2, 3, 4$ at three different resolutions $N_\theta = 16, 20, 24$. Right: “old” $(\hat{\theta}, \hat{\phi})$ -coordinates given in the new (θ, ϕ) -coordinates.

the following area and central n -moments of the curvature $n\sqrt{\mu_n(\bar{\mathcal{R}})}$:

$$\begin{aligned} A/4\pi &= 0.999285, & 2\sqrt{\mu_2(\bar{\mathcal{R}})} &= 0.280044, \\ 3\sqrt{\mu_3(\bar{\mathcal{R}})} &= 0.197685, & 4\sqrt{\mu_4(\bar{\mathcal{R}})} &= 0.342832, \end{aligned}$$

where

$$\mu_n(\bullet) := \langle \langle (\bullet) - \bullet \rangle^n \rangle,$$

and $\bar{\mathcal{R}} = c\mathcal{R}$ with $\langle \bar{\mathcal{R}} \rangle = 1$. As shown in fig. (2) (left) the scalar curvature significantly differs from that of a round sphere initially, where $\sigma = 0$ is set, but smoothes out towards $\mathcal{R} \approx 2$ in the Ricci flow (right), where we employ the relaxation method as explained in the last section. The fall-off is exponential, see fig.(3) (left), until it reaches a plateau of truncation error which converges to zero by increasing the spherical resolution. The second order scheme is computationally more efficient, since the parabolic flow is stable up to $\nu = 0.11$ for RK2-Heun and up to $\nu = 0.16$ for RK4⁷(measured for $N_\theta = 16$, $dx = 0.186$).

During the Ricci flow the surface area ($A/(4\pi) = 0.999285$) is bound but not fixed through eq.(25). The resulting round sphere metric $e^{-2\sigma}q_{ij}$ has the total area of $A/(4\pi) = 1.007889$, which we normalise to unity. In the next step, we compute the $l = 1$ eigenfunctions n^j of this metric, as explained in Sec. 3.4. As initial data for the relaxation method we picked $n^j|_{t=0} = \hat{n}^j$, where the parabolic flow was stable up to $\nu = 0.23$ for RK2. The three steady-state solutions are orthonormalised through the Gram-Schmidt process and inverted $n^j(\hat{n}) \rightarrow \hat{n}^j(n)$ using Newton-Raphson’s method (since we have access to $\partial_i n^j$). In fig. (3) (right) the old spherical coordinate lines $\hat{n}^j(n)$ are shown on the new grid on which we re-evaluate σ / the spherical round metric ${}^0q_{ij}$. The round metric in the canonical coordinates n^i can be embedded into Euclidean

⁶ $Re[\mathcal{N}_{1,2,3}] = 1/\sqrt{434}(-9, 17, -8)$, $1/\sqrt{3786}(-1, -43, 44)$, $1/\sqrt{78}(7, -2, -5)$ and $Im[\mathcal{N}_{1,2,3}] = -1/\sqrt{3}(1, 1, 1)$.

⁷ On the same surface solving the heat equation we got $\nu = 0.20$ RH2-Heun, $\nu = 0.28$ RH4.

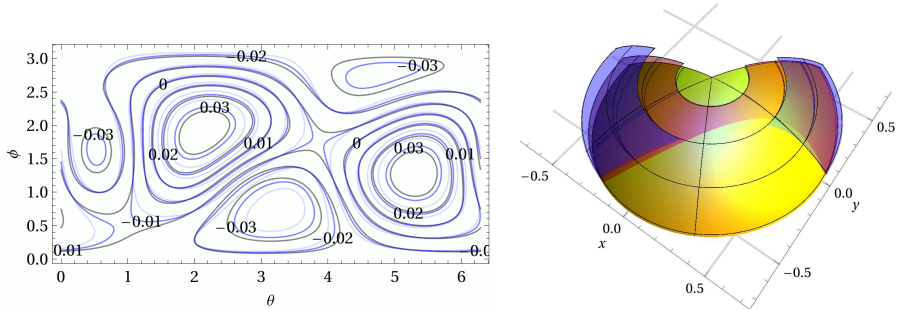


Figure 4: Left: Contours of difference $h_{(n+1)} - h_{(n)}$ between consecutive shape functions $h_{(n)}$ for $n = 1, 2, 3$ in embedding flow (black 3-2, blue 2-1, light blue 1-0). Right: Embedding flow at $t_{n=0,2,3} = 0.0, 0.66, 1.0$ (outer-transparent, inner-transparent, inner-solid).

space by the shape function $h_0 = 1$. During the embedding flow the shape is stepwise 'deformed' into the target shape function by solving the LEE at each step. Again the relaxation method with RK2 for $\nu = 0.2$ is employed.

We choose a conformal factor that is linear in t then the change of $h_{(n)}$ during the first steps of the flow $n = 1, 2, 3$, $t_{n=0,1,2,3} = 0.0, 0.33, 0.66, 1.0$. It is about linear in t as well which can be seen in fig. (4) (left); the difference between consecutive shape functions is approximately constant along a fixed direction. The increase/decrease is strongest in the directions where the target metric differs the most from the round metric. This is also apparent in fig. (4) (left) and fig. (6), where the embeddings of $q(t, \sigma)_{ij}$ at different states of the flow are shown. The drifting of grid points as illustrated in fig. (1) is not visualised but it can be seen how the unit sphere stepwise morphs into the target shape. The difference between $h_{(3)}$ and the original shape function, see fig. (6), is about 10^{-2} ; in order to refine the solution further we recursively apply the LEE, whereby d_{ij} the difference between target metric and induced metric as well as the intrinsic curvature converges exponentially with increasing n and increasing resolution, limited by a plateau of truncation error, see fig. (7). Note that due to the non-uniqueness of the embedding the final shape function is arbitrarily shifted and rotated wrt to the original one. In fig. (7) (left) the L_2 -norm in each l -eigenspace is shown. It is independent of rotations but not of the shifts, which is clearly visible in the different $l = 1$ modes.

5 Conclusion

In this article we presented a new numerical algorithm to solve the Weyl problem. The basic idea stems from the method of continuity which served as an

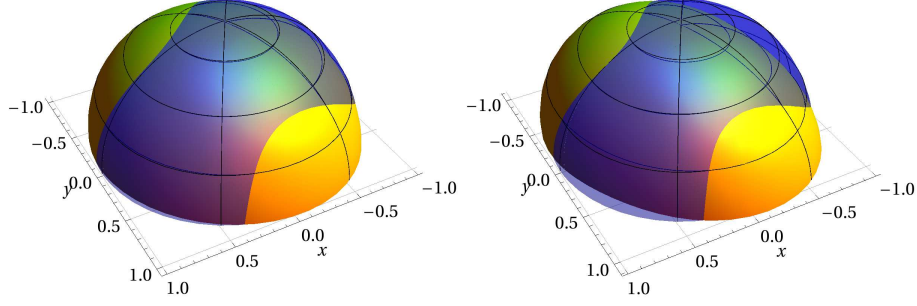


Figure 5: Embedding flow around unit sphere (transparent) at $t_1 = 0.33$ (left) and $t_3 = 1$ (right)

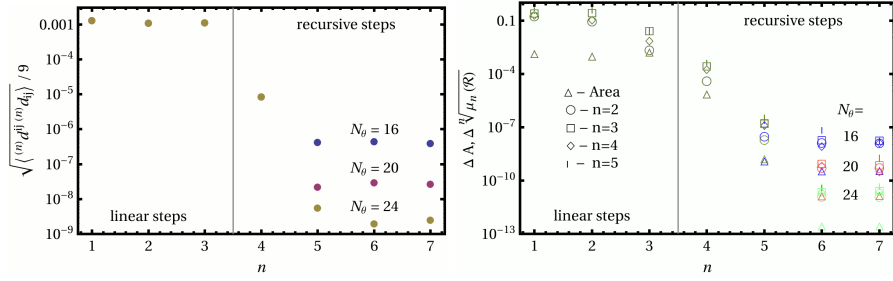


Figure 6: Left: Difference between the flow and the induced metric at linear $t_{n=1,2,3} = 0.33, 0.66, 1$ and recursive iteration $t_{n=4-7} = 1$ of the embedding flow. Right: Difference of the area A and $\mu_n(\mathcal{R})$ between the induced and target metric.

approach in Nirenberg’s proof of the conjecture and goes back to Weingarten and Weyl. The linearized embedding equations play a central role. They can be reduced to a single linear elliptic PDE by variable transformations. Solving the LEE stepwise for two ‘nearby’ metrics on a known embedding of one of the metrics allows one to ‘slowly’ deform an initial shape into the desired embedding (embedding flow). In doing so, it is necessary to link the target metric to an initial metric, whose embedding into \mathbf{R}^3 is known. For this purpose the round metric is well suited which is a steady-state solution of the Ricci flow on S^2 that can be evolved from any metric. But it is then in general given in arbitrary coordinates.

Hence, apart from solving the embedding equations, a number of additional obstacles appear, which complicates a numerical implementation of the method of continuity, namely we need to find a suitable coordinate system, solve various (non)-linear elliptic PDEs, (anti)-differentiate functions on the surface, handle

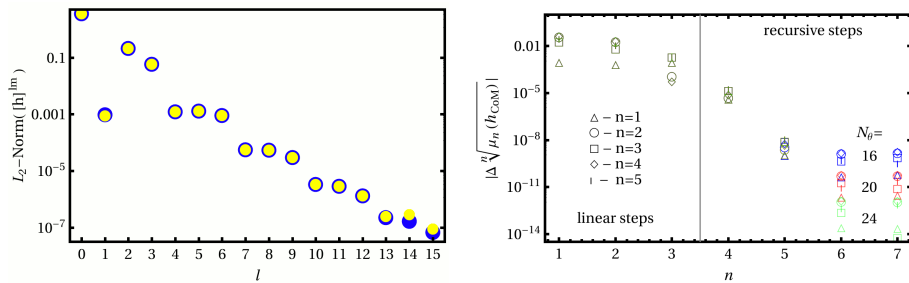


Figure 7: Left: L_2 -norm: $\sqrt{\sum_{m=-l}^l ([h]^{lm})^2}$ for original shape function h and $h_{n=7}$ for $N_\theta = 16$. The difference for higher modes and $l = 1$ is apparent. Right: Difference between the centered original and final shape function's μ_n converges with increasing resolution and flow time down to truncation error.

the drifting of grid points under the embedding flow or the $SO(3, 1)$ freedom of the solution etc. Another challenge is to keep the total numerical error of all steps small.

Through the use of over-determined quasi-Cartesian coordinates on the surface as well as spectral methods and the parabolic flow relaxation method we have shown how to overcome these technical difficulties altogether without losing numerical accuracy. Note that the compatibility with the simulations in $(3 + 1)$ numerical relativity is automatically given, since our approach requires as input an arbitrary shape function as well as a Riemannian 3-manifold, both of which generate an admissible 2-metric on the S^2 surface. This allows direct applications in binary black hole simulations to measure quasi-local mass or to investigate the large-scale dynamics of numerical simulations of inhomogeneous cosmological models, where the coarse-graining process involves solving the isometric embedding problem. These quasi-local mass definitions, like the Brown-York or the Kijowski-Liu-Yau mass [11, 3, 4, 14], are based on the comparison principle: anchor the intrinsic geometries by isometric embeddings and compare the extrinsic geometries. Moreover, isometric embeddings are ideal for visualising 2-metrics because they are fixed by unique shapes in the Euclidean space.

We have implemented our method with Fortran90 and tested it on a concrete arbitrarily chosen initial shape function in the Euclidean space. By direct comparison between the final and initial shape functions and metrics we were able to demonstrate exponential convergence by increasing the spherical resolution as well as the number of recursive iteration steps of the embedding flow. Our method is limited to positively curved and positive-definite 2-metrics and to ones whose isometric embedding and shape function in \mathbf{R}^3 is 'well represented' through harmonic polynomials within $l_{\max} < 40$, i.e. whose spherical harmonics power spectrum drops quickly enough, but is then guaranteed to reach a solution at reasonable computational costs, a few minutes on a modern CPU.

Apart from the applications already mentioned the numerical methods in the

sub-steps of our approach, like the implementation to solve the Ricci-flow or the $l = 1$ EV problem could lead to other applications in numerical relativity on their own. For example, to solve other elliptic PDEs that appear to find approximate Killing vector fields on trapping horizons [7] or to correct the gravitational waves signal of binary black hole simulations that is commonly extracted on coordinate spheres at finite radius. In general the spherical coordinates are distorted wrt the $l = 1$ eigenfunctions of these spheres. Furthermore, there are quasi-local mass and momentum measures, see [20] and references therein, which require isometric embeddings into Minkowski space (and into \mathbf{R}^3 as a sub-step) that would allow one to measure the linear momentum in numerical BBH simulation quasi-locally.

MK would like to thank Lars Andersson and Luciano Rezzola for their invitation to the Max Planck Institute for Gravitational Physics in Potsdam, which has enabled us to continue collaborating on this project. MJ thanks Badri Krishnan, Alex Nielsen, Frank Ohme and Joachim Friebe for helpful comments and discussions. This work was supported by the IMPRS for Gravitational Wave Astronomy in the Max Planck Society.

A Removing the positive eigenvalue from the spectrum of \mathcal{L}

In the code we solve equation (16) by relaxation method. This requires the linear operator \mathcal{L} to be non-negative. This is not the case because of the positive second term in (17). \mathcal{L} a positive principal eigenvalue λ_0 but can be modified \mathcal{L} to push that eigenvalue to the negative part of the spectrum. If the surface is not very far from a round sphere, we may expect that the spectrum of \mathcal{L} will not be very different from the one of $\Delta + 2$, and in particular will contain *only one* positive eigenvalue. In fact, our numerical evidence supports the conjecture that it is always the case for a convex surface.

The eigenfunction corresponding to λ_0 is not known, so the modification of \mathcal{L} is not completely trivial. First we define a new self-adjoint operator $\tilde{\mathcal{L}}$ as

$$\tilde{\mathcal{L}}(w) = \frac{1}{\sqrt{\mathcal{K}}} \mathcal{L} \left(\frac{w}{\sqrt{\mathcal{K}}} \right), \quad (28)$$

with \mathcal{K} denoting the trace of K_{AB} (we assume K_{AB} is negative definite). Since $\sqrt{\mathcal{K}}$ is positive everywhere, the dimensionality of subspaces where $\tilde{\mathcal{L}}$ is positive, negative or zero is the same as in \mathcal{L} . In particular, $\tilde{\mathcal{L}}$ has only one positive eigenvalue, which is non-degenerate. One checks straightforward that $\tilde{\mathcal{L}}(\sqrt{\mathcal{K}}) = \sqrt{\mathcal{K}}$, so this eigenvalue and the corresponding function are known explicitly. We now modify \mathcal{L} further by defining

$$\hat{\mathcal{L}}(g) = \tilde{\mathcal{L}}(g) - \frac{C}{\langle \sqrt{\mathcal{K}}, \sqrt{\mathcal{K}} \rangle} \langle \sqrt{\mathcal{K}}, g \rangle \sqrt{\mathcal{K}} \quad (29)$$

for a constant $C > 1$. It has the only positive eigenvalue shifted to the negative part of the spectrum and thus can be tackled by the relaxation method. Namely, the parabolic equation

$$\dot{f} = \widehat{\mathcal{L}}(f) - \frac{\tau}{\sqrt{\mathcal{K}}} + \frac{C}{\langle \sqrt{\mathcal{K}}, \sqrt{\mathcal{K}} \rangle} \left\langle \sqrt{\mathcal{K}}, \frac{\tau}{\sqrt{\mathcal{K}}} \right\rangle \sqrt{\mathcal{K}}, \quad (30)$$

converges to the solution of (16) divided by $\sqrt{\mathcal{K}}$. We can simplify (30) further by introducing a new variable $u = \frac{f}{\sqrt{\mathcal{K}}}$ which then (30) becomes

$$\dot{u} = \frac{1}{\mathcal{K}} (\mathcal{L}(u) - \tau) - \frac{C}{\langle \sqrt{\mathcal{K}}, \sqrt{\mathcal{K}} \rangle} \langle 1, \mathcal{L}(u) - \tau \rangle. \quad (31)$$

u tends exponentially to a solution of (16). We have found out that this also holds true if we simplify this formula by replacing $C/\langle \sqrt{\mathcal{K}}, \sqrt{\mathcal{K}} \rangle$ by a sufficiently large, positive number.

B Anti-differentiating a function in spherical harmonics

In Section 2.3 we show that the vector field Y^i can be reconstructed from its derivatives on the sphere. This leads us to the following numerical problem: Given the gradient of a function on S^2 expanded in terms of spherical harmonics, what is the spherical harmonics decomposition of the original function?

Let f be a function expanded in terms of Y^{lm}

$$f = \sum_{l=0}^{+\infty} \sum_{m=-l}^{m=l} Y[f]^{lm} Y^{lm}. \quad (32)$$

The ϕ derivative is

$$f_{,\phi} = \sum_{l=0}^{+\infty} \sum_{m=-l}^{m=l} Y[f]^{lm} im Y^{lm}, \quad (33)$$

so for all coefficients with $m \neq 0$ we obtain a straightforward relation between the expansions of f and $f_{,\phi}$:

$$Y[f]^{lm} = -\frac{i}{m} Y[f_{,\phi}]^{lm}. \quad (34)$$

In general the θ derivative of a regular f has a discontinuity at $\theta = 0, \pi$. This can be cured by multiplying it by $\sin \theta$. It is easy to see that $\sin \theta \frac{\partial}{\partial \theta} Y^{l,m}$ can be expressed in terms of other spherical harmonics with the same m . In particular, the harmonics with $m = 0$ satisfy

$$\sin \theta \frac{\partial}{\partial \theta} Y^{l,0} = \frac{l(l+1)}{\sqrt{(2l+1)(2l+3)}} Y^{l+1,0} + \frac{l(l+1)}{\sqrt{(2l-1)(2l+1)}} Y^{l-1,0}. \quad (35)$$

This equation gives us a recurrence relation for the $m = 0$ coefficients of f in terms of $\sin \theta \frac{\partial f}{\partial \theta}$

$$Y[f]^{l,0} = -\frac{\sqrt{(2l-1)(2l+1)}}{l(l+1)} Y[\sin \theta f, \theta]^{l-1,0} + \frac{(l-1)(l-2)}{l(l+1)} \sqrt{\frac{2l+1}{2l-3}} Y[\sin \theta f, \theta]^{l-2,0} \quad (36)$$

valid for $l \geq 2$. For $l = 1$ the relation reads

$$Y[f]^{1,0} = -\frac{\sqrt{3}}{2} Y[\sin \theta f, \theta]^{0,0}. \quad (37)$$

Finally the $Y[f]^{0,0}$ coefficient is arbitrary. This corresponds to the possibility of adding a constant to the solution.

References

- [1] A. D. Alexandrov. Existence of a polyhedron and of a convex surface with a given metric. *Doklady Akademii Nauk S. S. S. R.*, 50:103–106, 1941.
- [2] Mihai Bondarescu, Miguel Alcubierre, and Edward Seidel. Isometric embeddings of black hole horizons in three-dimensional flat space. *Classical and Quantum Gravity*, 19:375, 2002.
- [3] J.David Brown and Jr. York, James W. Quasilocal energy in general relativity. 1991. In *Mathematical Aspects of Classical Field Theory*, edited by Mark J. Gotay, Jerrold E. Marsden, and Vincent Moncrief (American Mathematical Society, Providence, 1992) pages 129–142.
- [4] J.David Brown and Jr. York, James W. Quasilocal energy and conserved charges derived from the gravitational action. *Phys.Rev.*, D47:1407–1419, 1993.
- [5] H. D. Cao, B. Chow, S. C. Chu, and S. T. Yau, editors. *Collected papers on Ricci flow*, volume 37 of *International Press Series in Geometry and Topology*. International Press, Somerville, Massachusetts USA, 2003.
- [6] B. Chow. The Ricci flow on the 2–sphere. *Journal of Differential Geometry*, 33:325–334, 1991.
- [7] Gregory B. Cook and Bernard F. Whiting. Approximate Killing Vectors on S^{*2} . *Phys.Rev.*, D76:041501, 2007.
- [8] Richard Hamilton. The Ricci flow on surfaces. *Mathematics and General Relativity, Contemporary Mathematics*, 71:237–261, 1988.
- [9] Qing Han and Jia-Xing Hong. *Isometric Embedding of Riemannian Manifolds in Euclidean Spaces*. American Mathematical Society, 2006.

- [10] Michael Jasiulek. A New method to compute quasi-local spin and other invariants on marginally trapped surfaces. *Class.Quant.Grav.*, 26:245008, 2009.
- [11] Jerzy Kijowski. A simple derivation of canonical structure and quasi-local hamiltonians in general relativity. *Gen. Relat. Grav. Journal*, 29:307, 1997.
- [12] Mikołaj Korzyński. Coarse-graining of inhomogeneous dust flow in General Relativity via isometric embeddings. *AIP Conf. Proc.*, 1241:973–980, 2010.
- [13] Mikołaj Korzyński. Covariant coarse-graining of inhomogeneous dust flow in General Relativity. *Class. Quant. Grav.*, 27:105015, 2010.
- [14] Chiu-Chu Melissa Liu and Shing-Tung Yau. Positivity of Quasilocal Mass. *Phys.Rev.Lett.*, 90:231102, 2003.
- [15] Louis Nirenberg. The Weyl and Minkowski problems in differential geometry in the large. *Communications on pure and applied mathematics*, 6:337–394, 1953.
- [16] Hans-Peter Nollert and Heinz Herold. Visualization in curved spacetimes. ii. visualization of surfaces via embeddings. In *Relativity and Scientific Computing*, pages 330–351. Springer-Verlag, Berlin, Heidelberg, 1996.
- [17] A. V. Pogorelov. On the proof of Weyl’s theorem on the existence of a closed analytic convex surface realizing an analytic metric with positive curvature given on the sphere. *Uspekhi Matematicheskikh Nauk*, 32, 1949.
- [18] Michael Spivak. *A Comprehensive Introduction to Differential Geometry*, volume 5. Publish or Perish, Berkeley, 1979.
- [19] László B. Szabados. Quasi-local energy-momentum and angular momentum in gr: A review article. *Living Reviews in Relativity*, 7(4):10, 2004.
- [20] M.-T. Wang and S.-T. Yau. Isometric Embeddings into the Minkowski Space and New Quasi-Local Mass. *Communications in Mathematical Physics*, 288:919–942, June 2009.